FRS Study of the Diffusion of a Block Copolymer. 1. Direct Determination of the Anisotropic Diffusion of Block Copolymer Chains in a Lamellar Microdomain

Dietmar Ehlich, Mikihito Takenaka, Shigeru Okamoto, and Takeji Hashimoto*

Department of Polymer Chemistry, Kyoto University, Kyoto 606, Japan

Received June 3, 1992; Revised Manuscript Received October 5, 1992

ABSTRACT: We discuss the applicability of forced Rayleigh scattering (FRS) as a means of a direct determination of possible diffusional anisotropies on the block copolymer systems with lamellar morphology. We report a first result which directly indicates the anisotropy of diffusion in this system. For this purpose the diffusion measurements were conducted on a bulk poly(styrene-*block*-isoprene) copolymer (M_n = 2.12 × 10^4) in the ordered state and in directions parallel and perpendicular to the surface of an oriented film at temperatures higher than the glass transition temperature of polystyrene microdomains.

I. Introduction

Block copolymers are interesting compounds from structural and from dynamical points of view, because in general when their temperature or concentration is changed, they undergo an order–disorder transition (ODT) which is regarded as a liquid–liquid phase transition. The phase transition induced below ODT develops specific geometrical and topological patterns known as microdomains, which should give rise to a characteristic transport behavior. The two most general features of this microscopic order in regard to transport properties are *anisotropy* and *confinement*. Both phenomena can appear independently. Anisotropic diffusion without confinement is well-known from the mobility in single-crystal materials. Confinement restricts the diffusion onto a euclidian or fractal subspace of dimension smaller than 3 and will induce anisotropic motion only if this subspace is anisotropic. Confinement can be absolute or partial depending upon the probability for a diffusion molecule to leave this subspace. These effects may be expected to appear in the motion of probes, but the most striking effect is expected for the motion of the block copolymers themselves. In lamellar block copolymers, one expects a more or less strongly confined mobility of the copolymer chains perpendicular to the lamella interfaces due to the segregation power which causes the ODT and conserves the stability of the microdomain structure, while the diffusion inside the lamella parallel to their interfaces is expected to be less confined. Some first indirect proof of the confinement in the self-diffusion of a bulk lamellar block copolymer has recently been published.[1] The theory concerning the diffusion in block copolymer systems[2] is still rather scarce.

However, any experiments have to deal with a macroscopic sample, and hence macroscopic alignment of the microdomains becomes pivotal. Generally, the methods to obtain macroscopically anisotropic samples of a lamellar block copolymer, e.g., solvent casting[3] or the application of shear,[4] lead to films with lamellar microdomains with a long-range spatial order, having their interfaces oriented preferentially parallel to the film surface.

The main advantage of forced Rayleigh scattering (FRS) is that, by including the reflection geometry (see Figure 1b), some diffusional anisotropy can be detected in a once-prepared sample just by differently orientating this sample (film or slab) relative to the laser beams, as shown in Figure 1. This method is less ambiguous than the conventional method for characterizing the diffusional anisotropy in a

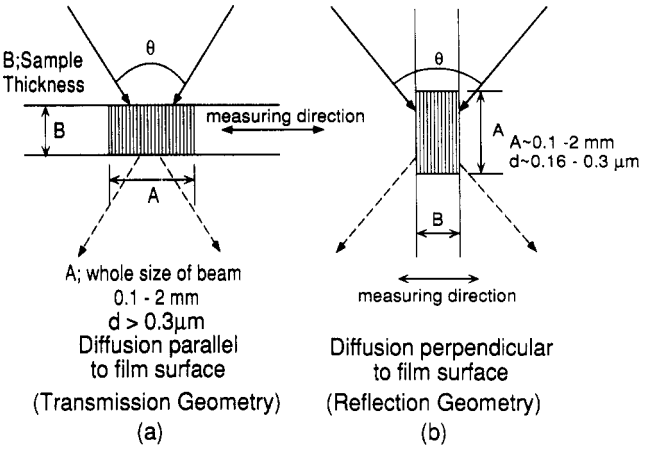

Figure 1. Measurement condition for FRS: (a) transmission geometry and (b) reflection geometry.

sense that one can avoid experimental errors associated with the procedures to prepare two sets of specimens for the diffusion measurements parallel and perpendicular to the film surface. Especially for the diffusion experiments parallel to the sample surface, one may have to use a complicated specimen preparation: one has to stack first many oriented films onto each other and compound them to a new specimen to obtain a sufficient width of the specimen in a direction normal to the film surface, and then one has to prepare a thin slab by cutting this new specimen perpendicular to the original sample surface. Of course the structure and its orientation in the original film has to be maintained in the process of preparing this thin slab, which is not necessarily easy. On the other hand, the diffusion experiments normal to the sample surface may be rather straightforward and can be performed with the original film or the compound specimen.

There is one limitation for FRS because, in the most interesting case of reflection geometry where diffusion perpendicular to the film surface can be measured (Figure 1b), the fringe spacing is limited to values below about 300 nm due to geometrical constraints of the sample holder and the physical limit of total reflection. Likewise there is a limitation of the fringe spacing above about 300 nm for the transmission geometry (see Figure 1a).

II. Experimental Section

1. Material. The synthesis and characterization of poly(styrene-*block*-isoprene) (SI) block copolymer used in this

0024-9297/93/2226-0189$04.00/0

experiment was described in detail elsewhere.[5] The number-average molecular weight M_n of the block copolymer was obtained by membrane osmometry in toluene ($M_n = 2.12 \times 10^4$) and $M_w/M_n = 1.07$ from GPC, where M_w is the weight-average molecular weight. The polystyrene (PS) content of 42 wt % was obtained from the molecular weight of the PS precursor as measured with GPC. The block copolymer was fractionated in a preparative GPC column to eliminate homopolymer as well as the AB–BA triblock copolymer formed as a recombination product on functional termination. The block copolymer was chemically labeled with the photosensitive (irreversible) FRS dye 2-nitro-4-carboxy-4'-(dimethylamino)stilbene (ONS).[5] Using the UV–vis absorption of the ONS dye, the labeling efficiency was determined to be 60%.

The films specimens for the FRS measurements were prepared as follows. A powdery precipitate of the block copolymer was first cold-pressed between metal plates. The film specimen thus obtained was then hot-pressed at about 150 °C (in the ordered state) between two glass plates into the sample of 10 mm in diameter, and the film thickness was adjusted to 50–100 μm by use of Teflon spacers. The biaxial flow occurring during the hot-pressing process leads to a strong preferential orientation of the lamellae with their interfaces parallel to the film surface.[6] The orientation of lamellae is, however, essentially random within a plane parallel to the film surface.

2. SAXS and TEM. The small-angle X-ray scattering (SAXS) has been performed with a Rigaku rotating-anode X-ray generator (Cu Kα line, 0.154 nm in wavelength), graphite monochromator, and point collimation and an imaging plate[7] as a two-dimensional X-ray detector or slit collimation and a position-sensitive proportional counter (PSPC) as a one-dimensional detector. Details of the detector will be described elsewhere.[7] Samples for SAXS were prepared by stacking about 30 of the 50-μm-thick films as prepared for FRS measurements to form a macroscopic sample of about 1.5 × 3 × 10 mm³ size. Two-dimensional (2D) patterns were taken at room temperature using the imaging plate in "edge-view", and "through-view", i.e., with the incident X-ray beam parallel and perpendicular to the film surface, respectively. The ODT of this sample has been determined to occur at 190 ± 5 °C independently by measuring the SAXS profiles as a function of temperature.[5,8]

Ultrathin sections for transmission electron microscopy (TEM) were stained with osmium tetraoxide according to standard procedures.

3. FRS. Diffusion measurements were performed with a newly constructed FRS setup[5] using different fringe spacings between 0.17 and 14.0 μm. An argon ion laser (NEC GLG3200) in single-mode operation at a 488-nm wavelength was used as a light source for bleaching and for reading as well, for which the beam intensity was attenuated by a factor of 10^3–10^4. Measured intensities are normalized on the incident intensity of the laser beam which was monitored continuously to correct for intensity fluctuations due to mode hopping, etc. All measurements were carried out under a nitrogen atmosphere to eliminate the thermal oxidation of the ONS dye. With this procedure the samples became completely colorless after bleaching; no isatogene was formed.[9] The measurements were performed in transmission and reflection geometry as explained in Figure 1. The two orthogonal orientations of the sample relative to the two laser beams permit the study of the diffusion parallel and perpendicular to the sample surface, respectively. The fringe spacings were calculated from the light wavelength and the angle of intersection between the two laser beams according to the Bragg equation. For reflection geometry the refractive index of the sample is relevant for determining the fringe spacing. It was assumed as $n = 1.44$, an average value of PS and PI. The FRS signal decay was fitted with a sum of two exponential functions according to[10]

$$I(t) = [A_1 \exp(-t/\tau_1) + A_2 \exp(-t/\tau_2) + B]^2 + C \qquad (1a)$$

In eq 1a, A_1 and A_2 denote the amplitudes, τ_1 and τ_2 are the relaxation times, B is the coherent background, and C is the incoherent background originating from light scattered by dust, the glass surfaces, etc. B and C can be determined by measuring the light scattered from the specimens before bleaching (C) and after the FRS signal decay has ceased ($B^2 + C$). These values were measured, and B was found to be negligible, i.e.

$$I(t) \cong [A_1 \exp(-t/\tau_1) + A_2 \exp(-t/\tau_2)]^2 + C \qquad (1b)$$

It is important to note that the fitting with the two exponential decay functions does not mean at all that there are two physically distinct decay processes but rather means that there is a distribution of decay times which is narrow enough to be fitted to the double-exponential functions.

All samples were annealed 3 days prior to measurement.

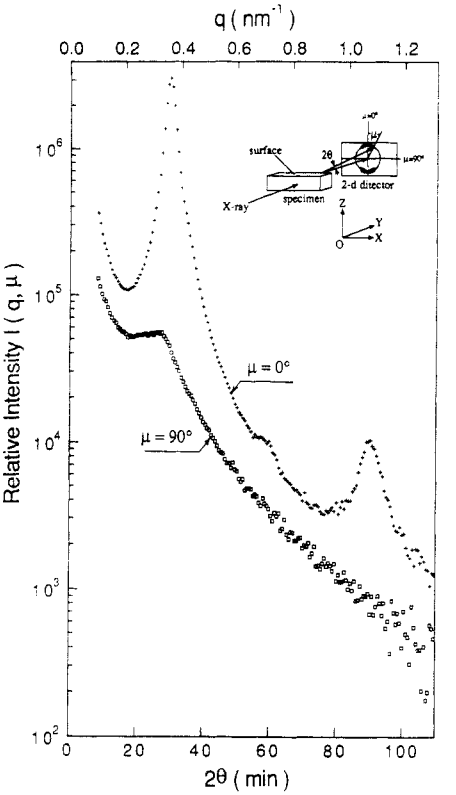

Figure 2. SAXS intensity profiles plotted as a function of the scattering angle 2θ or the magnitude of the scattering vector q at $\mu = 0°$ and $\mu = 90°$.

III. Experimental Results

Figure 2 shows the SAXS intensity distributions from the specimens at room temperature taken with the imaging plate as a two-dimensional detector. The 2D pattern was taken in the edge-view configuration. The logarithms of the relative intensities in the direction normal ($\mu = 0°$) and parallel ($\mu = 90°$) to the surface of the film specimens were plotted as a function of scattering angle 2θ(min). In the meridional intensity distribution, $I(2\theta,\mu=0°)$, the first- and third-order Bragg peaks can be clearly seen, while the second-order peak is suppressed and appears only as a shoulder. This is due to coincidence of the second-order peak in the lattice factor with a minimum in the particle form factor, which is expected for a block copolymer having alternating lamellar microdomains with almost symmetrical volume.[11] The equidistant position of the Bragg peaks corresponds to a lamellar morphology with a domain spacing of 18.8 nm. This can also be confirmed directly in the TEM micrograph shown in Figure 4. The strong anisotropy in the intensity distribution $I(2\theta,\mu)$ as revealed by $I(2\theta,\mu=0°) \gg I(2\theta,\mu=90°)$ in Figure 2 corresponds to a preferential orientation of the lamellae with their interfaces parallel to the surface of the specimen films.

From the azimuthal angle (μ) dependence of the SAXS intensity, we estimated orientation distribution function $w(\beta)$ of lamellar normal $\mathbf{n}$, a unit vector normal to the

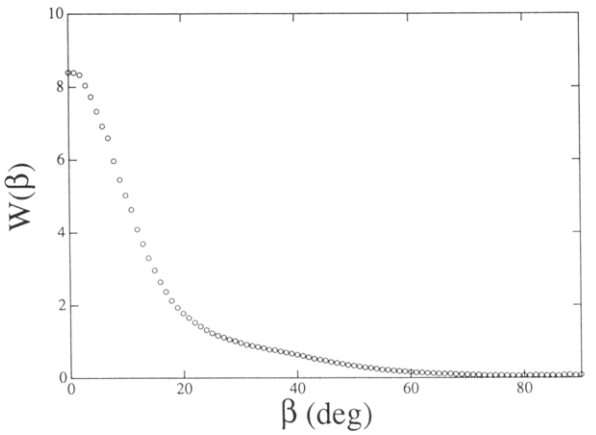

Figure 3. Normalized orientation distribution function $w(\beta)$ for the lamellar normal with respect to the film normal.

lamellar interface

$$w(\beta) \sin \beta \, d\beta = \frac{\int_{q_1}^{q_2} I(q,\mu=\beta) q^2 \, dq \sin \beta \, d\beta}{\int_{\beta=0}^{\pi} \int_{q_1}^{q_2} I(q,\mu=\beta) q^2 \, dq \sin \beta \, d\beta} \quad (2)$$

where q is the magnitude of the scattering vector defined by $q = (4\pi/\lambda) \sin \theta$ (λ is the wavelength of X-ray) and β is the angle between **n** and the z axis, the direction normal to the film surface. q_1 and q_2 are the q values at the lower and upper bounds of the measurements ($q_1 = 2.53 \times 10^{-1}$ nm^{-1} and $q_2 = 1.30$ nm^{-1}). The orientation order parameter f was estimated for **n**

$$f \equiv [3\langle \cos^2 \beta \rangle - 1]/2 \quad (3)$$

and

$$\langle \cos^2 \beta \rangle = \int_0^{\pi} w(\beta) \cos^2 \beta \sin \beta \, d\beta \quad (4)$$

The specimen used here was found to have $f = 0.35$. Figure 3 shows the orientation distribution function $w(\beta)$ thus determined.

The 2D SAXS pattern taken with the through-view configuration was very weak as expected from the ratio of $I(2\theta,\mu=90°)/I(2\theta,\mu=0°) < 0.1$ and was nearly circularly symmetric; the anisotropy was very weak if it existed. This is consistent with the results obtained from Figure 2; most of the lamellae are oriented with their **n** parallel to the OZ axis. Although a minor fraction of lamellae are oriented with their **n** perpendicular to the OZ axis, their **n** were essentially random in the plane of OXY (see Figure 2).

Figure 4 shows a TEM micrograph which has been taken from an 50-μm-thick film, the preparation of which was identical to that used in the SAXS and FRS measurements. The sample has been cut perpendicular to the film surface. From this image we can estimate the grain size to be typically in the range of some microns. At a length scale greater than the persistence length of the system (grossly 100 nm to 1 μm), the lamellae bend slightly, typically 30–40°. This bending is quite regularly alternating to both sides; thus, no significant backfolding of the lamellae can be observed.

In Figure 5 the intensity of the FRS signal decay at 112 °C has been plotted against time for measurements at different fringe spacings as indicated in the figure captions. This temperature is far below the ODT of the block copolymer so that we can assume that the block chains are segregated into respective microdomains. The incoherent background C according to eq 1 has been measured and is subtracted. The signal decay of the individual measurements occurs at very different times, due to the large variation in the diffusion length. To cover these large differences in time scale, the logarithm of the intensity has been plotted against the logarithm of time. In this plot, the quite gradually decreasing intensity visualizes that the decay is not single exponential. A sum of two exponentials is generally necessary to fit these data. However, we cannot assign these decay constants to two well-defined physical processes, which should reveal themselves in two separate steps in the decay function. The decay is extended quite homogeneously over a range of decay constants which is just narrow enough to make a description with two exponentials sufficient. Thus it seems to be more suitable to fit the intensity decay data by Laplace transformation

$$I(t) = [\int A(\tau) \, e^{-t/\tau} \, d\tau]^2 + C \quad (5)$$

although this is at present not yet feasible for us.

The filled symbols in Figure 5 correspond to diffusion measurements perpendicular to the film surface (the reflection geometry). In these measurements the signal intensity is not decaying completely, but a leveling off is observed at longer times. The absolute height of this constant or more accurately slowly decaying level, which amounts to a few percent of the initial intensity, is not

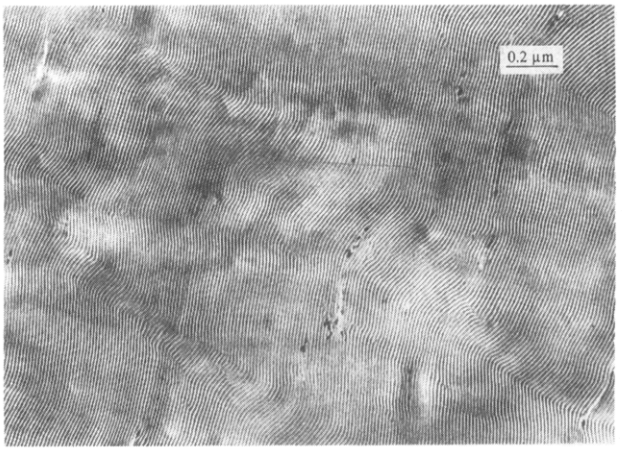

Figure 4. Transmission electron micrographs of the samples used for the FRS measurements.

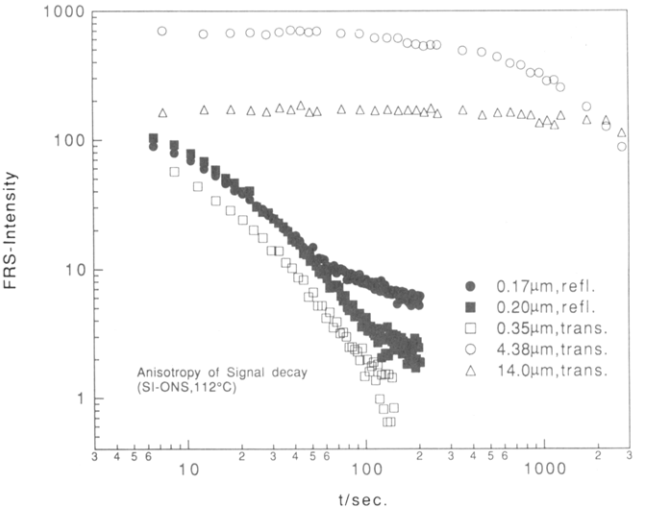

Figure 5. Time changes of the FRS intensity for measurements with various fringe spacings at 112 °C, in double-logarithmic scales. The filled and open symbols correspond to the measurements with the reflection geometry and transmission geometry, respectively.

very reproducible and varies quite strongly if the experiment is reproduced at different positions on the sample. However, it typically occurs for the measurements in reflection geometry, thus for the diffusion perpendicular to the film surface and hence perpendicular to the preferential orientation of the lamellar interface according to Figure 2. The slowly decaying level reflects a fraction of lamellae with their **n** parallel to the measuring direction. The fact that such a level amounts only to a few percent of the initial intensity can be understood, if we consider the waviness of the lamella interface as can be seen in Figure 4 together with the strong sensitivity of the effective diffusion constant on the tilting angle of the lamellar interface relative to the measuring direction, especially when the measuring direction is almost perpendicular to the lamellar interface. This will be discussed in more detail in section IV.

The variation of the signal decay time with the change of the fringe spacing proves that the signal decay is caused by a transport process. If the transport process obeys Fickian diffusion, we have

$$1/\tau = (4\pi^2/d^2)D \tag{6}$$

where D is the diffusion coefficient. Thus, if this is the case, the time scale for each FRS decay curve can be renormalized by dividing the time through d^2, the square of the fringe spacing. After this procedure all curves should fall on one master curve. In Figure 6a the FRS intensity corrected for the incoherent background C (eq 1) has been plotted logarithmically against t/d^2, where a relatively good master curve was obtained for the transmission geometry but not for the reflection geometry. For the reflection geometry, the component of the FRS signal which decays at a slower rate in eq 1b [e.g., $A_2 \exp(-t/\tau_2)$] seems to be very different for the two measurements with the different fringe spacings. To see this effect qualitatively, the slowly decaying component was assumed to be a constant coherent background level A_2 with $\tau_2 = \infty$, i.e.

$$I(t) \cong [A_1 \exp(-t/\tau_1) + A_2]^2 + C \tag{7}$$

and this level A_2 as well as C was subtracted by using eq 7 to obtain the FRS signal decay curves ${A_1}^2 \exp(-2t/\tau_1)$ corrected for A_2 and C in part b. The superposition of the decay curves after these corrections seems to be better in part b but is not still perfect.

The level A_2 in eq 7 exists for the two measurements in reflection geometry (filled symbols) as shown in part a. This level A_2 is much suppressed in transmission geometry compared with that in reflection geometry, as is naturally expected. The level A_2 under transmission and reflection geometries may reflect, in principle, the fractions of the lamellae whose interfaces are oriented normal and parallel to the film surfaces, respectively (Figure 1). Since the level A_2 is extremely sensitive to the relative orientation between the film normal and the measuring direction, it is practically difficult at present to interrelate the level A_2 and the particular lamellar orientation as discussed above. A very rigorous adjustment of the sample cell orientation is required for this purpose.

It should also be noted that the average orientation of the lamella within the hologram area changes from place to place in the specimen, as will be discussed later (section IV) in conjunction with an "intermediate scale experiment". In fact this is a primary reason why the reduced FRS decay curves obtained with different spacings at different beam spots do not superpose each other in parts a and b of Figure 6 or why the values τ_1 and τ_2 determined using eq 1b scatter much as will be shown in Figure 7.

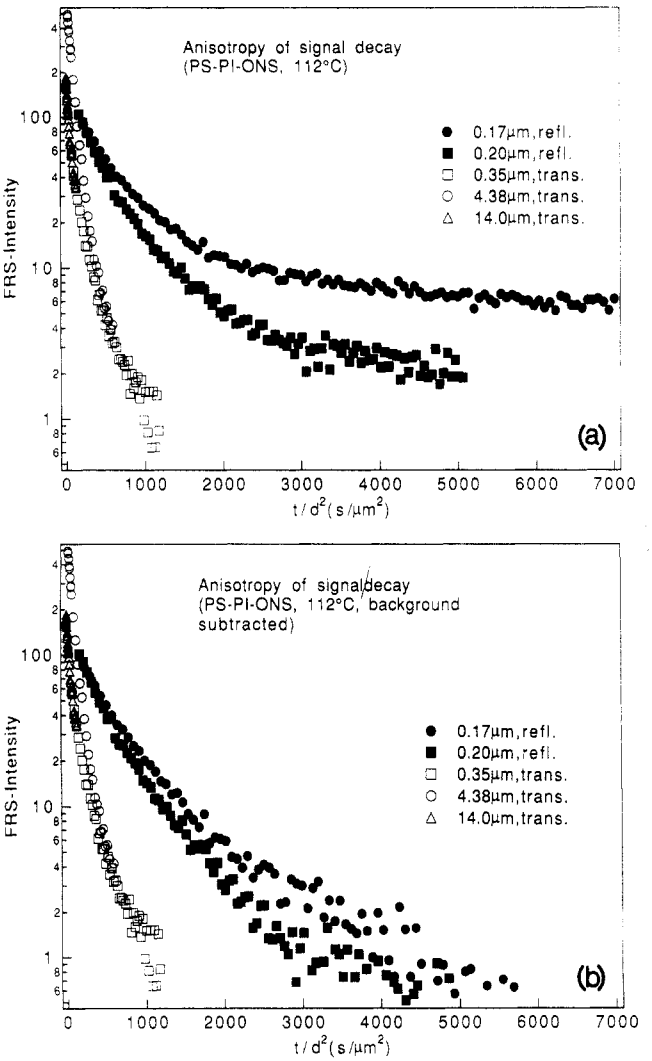

Figure 6. FRS intensity (a) without the subtraction and (b) with the subtraction of background plotted as a function of the reduced time t/d^2 at 112 °C where d is the fringe spacing. Symbols have the same significance as in Figure 5.

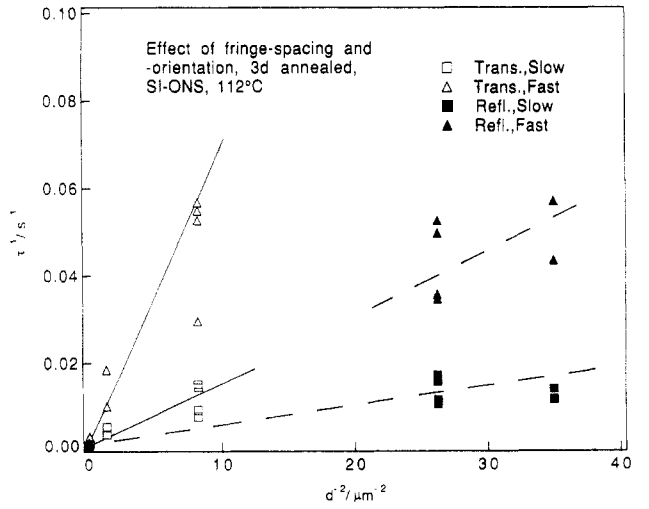

Figure 7. Reciprocal relaxation time plotted as a function of the reciprocal square of the fringe spacing at 112 °C. Symbols have the same significance as in Figure 5. Triangles and squares indicate the fast and slow decay components, respectively.

Obviously the measurements in transmission geometry (open symbols) overlay quite well to form a master curve as seen in parts a and b of Figure 6. All these measurements correspond to the diffusion parallel to the film surface. As the lamellar interface is oriented preferentially in this

direction we expect the quickest diffusion for this orientation. The change in fringe spacing from 0.35 to 14 μm does not lead to drastic deviations from the Fickian d^2 behavior, although the characteristic diffusion length thus changes from a value slightly below the estimated average grain size around 1 μm to a value above the average grain size. As will be discussed later in section IV, this is in harmony with the absence of backfolding as shown in the TEM micrograph in Figure 4. The measurements in reflection geometry reveal a much slower decay; thus, they show a much slower diffusion process perpendicular to the film surface. The slight difference between the two reflection measurements at 0.17 and 0.20 μm as seen before (Figure 6a) and after (Figure 6b) the subtraction of A_2 in eq 7 is due to the fact that each measurement has to be performed at a new spot on the sample and is not related to the difference in fringe spacing.

To estimate the corresponding diffusion coefficients, we have plotted in Figure 7 the reciprocal relaxation times as obtained from the fits of eq 1b against the reciprocal square of the fringe spacing based on eq 6. Four straight lines, two solid lines obtained for the transmission geometry, and two dashed lines obtained for the reflection geometry were drawn just to facilitate a quicker understanding of general trends. The open symbols correspond to transmission geometry while the filled symbols again show the behavior in reflection geometry. The triangles show the fast-decaying component of eq 1 and the squares the slowly decaying part. This plot is also sensitive to detect some contribution to the signal decay which is not caused by a transport process. It has to be applied, if the FRS label is reversible, to separate the thermal backisomerization of the label. We can show that no such nontransport contribution exists as the decay rate approaches zero when the fringe spacing becomes infinity. Thus the oxidation step of the ONS dye has been successfully suppressed by using the nitrogen atmosphere.[5]

Fickian diffusion should lead to a straight line in this plot (eq 6). However, as we found in non-single-exponential signal decay, the decay constants obtained from eq 1 are spread over some range in τ^{-1} for each fringe spacing. The values from the slow and fast components of eq 1 are not well separated but overlapping. This could be expected yet qualitatively from the signal decay in Figure 5 and has been discussed there. Therefore, it is only possible to determine some limiting diffusion constants for the fast and slow components. Yet it is obvious that the diffusion measurements in reflection geometry lead to strongly different diffusion coefficients than the measurements in transmission geometry. The fast-diffusion component in reflection geometry (filled triangles) is as quick as the slow-diffusion component in transmission geometry (open squares). We obtain diffusion coefficients of $D_{slow} \cong 3.86 \times 10^{-13}$ cm^2/s and $D_{fast} \cong 1.81 \times 10^{-12}$ cm^2/s parallel to the film surface and $D_{slow} \cong 1.19 \times 10^{-13}$ cm^2/s and $D_{fast} \cong 3.86 \times 10^{-13}$ cm^2/s perpendicular to the film surface.

A quantitative correlation of this anisotropy in a transport quantity with the structural anisotropy as determined by the two-dimensional SAXS measurement would be highly desirable. On the basis of present theories concerning the diffusion in confined systems as well as on the theory of forced Rayleigh scattering, however, it is not yet possible, as will be discussed in the next section.

IV. Theoretical Considerations

To interpret the FRS signals for a lamellar block copolymer, two steps have to be considered: (a) the time development of the long-range concentration fluctuation of labeled molecules which was created in the initial bleaching or writing step and subsequent self-diffusion of the labeled molecules and (b) the correlation of the FRS signal intensity at time t with this concentration pattern at the same time. We will call point (a) the "diffusion problem". It means in general to solve the Fickian diffusion equation with the bleached concentration pattern as starting condition under the constraints and specifics of the regarded physical system. The starting condition is only known approximately, but so far under the assumption of a concentration-independent diffusion coefficient, we only needed to look at the dominating Fourier component (first-order Bragg peak) onto which the detector is adjusted. We shall term point (b) as the "scattering problem". Here usually the results of the coupled wave theory for the diffraction from gratings are used.[12]

It will turn out that on the basis of current theories there are three types of experiments, which can be understood quantitatively, while there is as yet no possibility to treat the general case. To differentiate the types of experiments, it is helpful to look at the natural length scales. For the FRS method these are (i) the size of the interference fringes **d**, giving the distance over which molecular motion is observed and (ii) the integral size of the hologram **A**, i.e., that region in the sample from which the scattered light hits the detector, so that the amplitudes are summed up (see Figures 8, 9, and 11). The direction normal to the fringes is called the measuring direction because only molecular motions in this direction are effective for FRS.

While **d** is determined by the angle between the two partial beams, wavelength, and refractive index and thus known with an accuracy of a few percent, **A** can only be estimated coarsely using beam diameter, space beam overlap, and sample thickness. In a typical FRS experiment, **d** can be varied between 200 nm and about 20 μm; the beam diameter (spot size) is usually between 0.1 and 2 μm. These methodical scales have to be compared with the two characteristic scales of a lamellar block copolymer system, i.e., size of the domain **l** and size of the grain **L** (see Figures 8, 9, and 11). **l** is obtained by small-angle X-ray or neutron scattering and lies typically above 100 Å depending on the molecular weight and segregation power of the constituent block chains, while **L** may vary largely for a given polymer form **l** to almost macroscopic dimensions, depending on sample preparation condition. It can only be guessed from the degree of anisotropy in the SAXS pattern and the structure seen in electron micrographs.

If the lamellar orientation does not change over the whole beam diameter, we have $\mathbf{L} > \mathbf{A}$ which we shall term a "single grain" or "local scale" experiment (Figure 8). This local scale experiment allows the determination of the local motional anisotropy which can be described in terms of a diffusion tensor. Two of its main values are equal and describe the diffusion coefficient $\mathbf{D}_\parallel$ parallel to the lamellar plane. The third component describes the diffusion perpendicular to the lamellae $\mathbf{D}_\perp$ which is supposed to be much slower in cases of strong confinement. For simplicity we will assume it to be negligibly small compared with $\mathbf{D}_\parallel$. We expect an exponential FRS signal decay with relaxation time τ, and as we vary **d** in this range the usual $\mathbf{d}^2$ dependence of the decay constant should be observed, leading to a corresponding diffusion coefficient **D** as given by eq 6. Change of the measuring direction leads to a change in the decay constant, i.e., $\tau = \tau(\alpha)$, where α is the

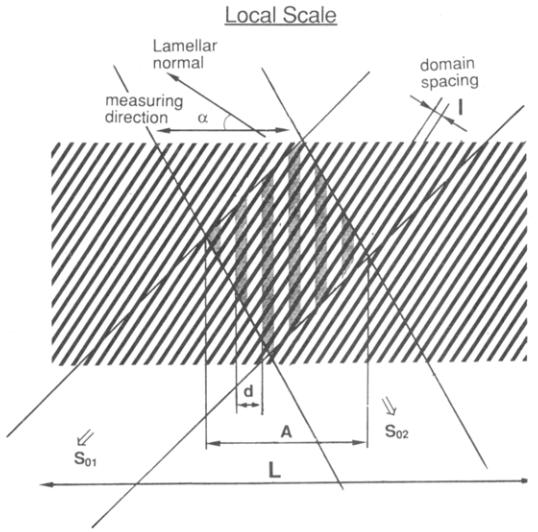

Figure 8. Schematic illustration of the local scale experiment satisfying $\mathbf{d} < \mathbf{A} < \mathbf{L}$. **d**, **A**, **l**, and **L** are the size of the interference fringes, the integral size of the hologram, the size of the domain, and the size of grain, respectively. Unit vectors $\mathbf{S}_{01}$ and $\mathbf{S}_{02}$ specify propagation directions of the partial beams generating the holographic fringes.

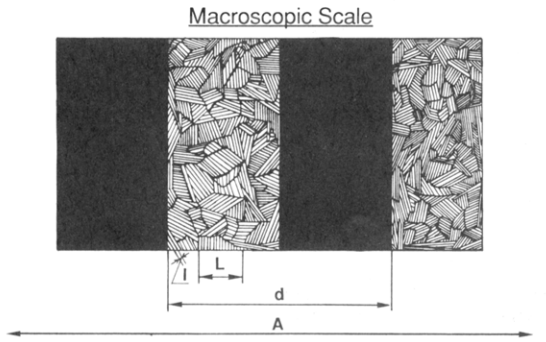

Figure 9. Schematic illustration of the macroscopic scale experiment, satisfying $\mathbf{L} < \mathbf{d} < \mathbf{A}$, where **d**, **A**, **l**, and **L** have the same significances as in Figure 8.

angle between the measuring direction and the normal to the lamellar interfaces. For the two extreme orientations we may obtain directly the local diffusion coefficients $\mathbf{D}_\parallel$ and $\mathbf{D}_\perp$. For arbitrary orientations the diffusion coefficient depends on the lamellar orientation as

$$\mathbf{D}(\alpha) = \mathbf{D}_\parallel \sin^2 \alpha + \mathbf{D}_\perp \cos^2 \alpha \cong \mathbf{D}_\parallel \sin^2 \alpha \qquad (8)$$

However, such a single grain experiment seems very difficult to realize, because one has to generate (and prove) a grain size of more than 100 μm, a lower limit for **A**.

At the other end of the scale, we have the "macroscopic scale" experiment (Figure 9), which requires $\mathbf{L} \ll \mathbf{d}, \mathbf{A}$. In this case we can assume a "coarse-grained" approach and treat the material as homogeneous but possibly still anisotropic, if the grains have some preferential orientation. In this case as well, we expect a single-exponential behavior with $\mathbf{d}^2$ behavior for the diffusional FRS decay (eq 6), the decay constant depending on the sample orientation if there is a preferential orientation of the grains and some motional anisotropy within the grains such as is the case for cylindrical and lamellar microdomains. The local diffusion coefficients are always lower and upper thresholds for the macroscopic diffusion coefficients. But the diffusion cannot be understood in terms of this local anisotropy and the orientation distribution of grains alone. This is because in general there is an additional grain-boundary effect compared to the local scale experiment.

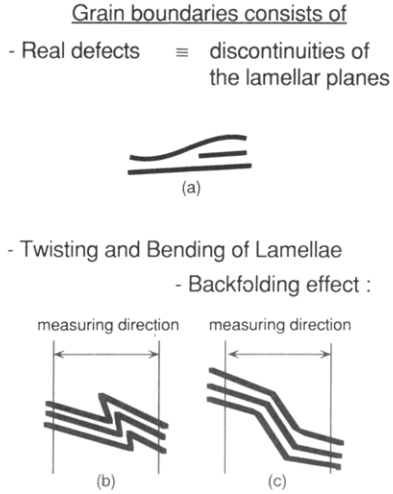

Figure 10. Illustration of some defects in lamellar microdomains.

If we picture the lamellar system not using grains but as continuous, folded interfaces, such grain boundaries can be characterized by the tortuosity and winding of these interfaces and furthermore by the spatial distribution of real defects in the continuity of the lamellae (Figure 10a). In the case of folded interfaces the grain size may be characterized by a persistence length ξ for the folded or curved interfaces. The length ξ may be regarded as a correlation distance for the orientation correlation function $f(\mathbf{r})$ for the two vectors $\mathbf{n}_1$ and $\mathbf{n}_2$ normal to the lamellar interface at a position vector **r** apart

$$f(\mathbf{r}) = [3\langle(\mathbf{n}_1 \cdot \mathbf{n}_2)^2\rangle_r - 1]/2 \qquad (9)$$

where $\langle X \rangle_r$ denoted an ensemble average of X at a given displacement vector **r**. It is important to note that the macroscopic diffusion coefficient is not fully determined, even in the case in which the orientation distribution of the grains and the distribution of the grain size are specified. This situation may be visualized, for example, in the case where the lamellae may be folded in two different ways to yield the same orientation as sketched in parts b and c of Figure 10. Such "backfolding" effects as sketched in Figure 10b may prolong the diffusional path along the measuring direction as indicated in the figure, relative to the folding shown in Figure 10c, and thus reduce the diffusion coefficient if a sample is prepared suitably. On a shorter length scale this will also lead to marked deviations from the $\mathbf{d}^2$ dependence of the signal decay.

The quantitative effect of this backfolding reduction of the diffusion depends on the real average path length one molecule has to move to produce one diffusional step in the coarse-grained picture and cannot be obtained from local interface properties, e.g., curvature alone. The suppression of the diffusion due to the interface curvature should be more pronounced in systems having a cylindrical domain type because of the two-dimensional confinement. The backfolding effect will be suppressed easily, however, if the diffusion perpendicular to the interface is no longer negligibly small.

The real defects, i.e., discontinuities, in the lamella interfaces will exist in all systems, especially after fresh preparation, and are supposed to diminish with time on annealing in the ordered state. It is difficult to predict their mobility and the mobility of single chains in their environment. However, approaching the equilibrium ordered state, they will become comparably rare, and as they are of low dimensionality, one can expect that they will influence diffusion only in their nearest neighborhood.

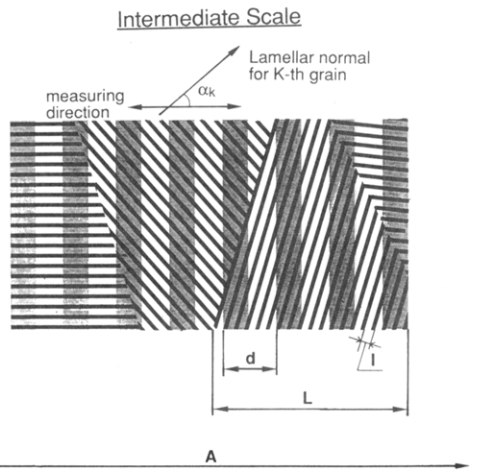

Figure 11. Schematic illustration of the intermediate scale experiment, satisfying **d** < **L** < **A**, where **d**, **A**, **l**, and **L** have the same significances as in Figure 8.

The macroscopic experiment can be realized. However, to measure diffusion perpendicular to the film surface is almost impossible in this region because for FRS the grains would have to be made significantly smaller than about 10 times *l*.

Between these two most easily understandable extreme cases, we can figure out a number of further experiments among which we shall consider the one termed "intermediate scale" experiment. We assume the grain picture, and we require **d** ≪ **L** ≪ **A** (Figure 11). This means we have many fringes inside each grain as well as many grains inside the hologram. Furthermore, we assume that the grain orientation does not change over the sample thickness but only laterally in the sample (see Figure 11). In this case grain-boundary effects are negligible and we can treat the experiment as a weighted sum of coherent local scale experiments.

The weighting factors are given by the orientation distribution of the grains if really **L** ≪ **A** is valid so that the average is taken over a representative area in the sample. As **A** and **L** approach each other more and more, each single experiment will measure only a mere subensemble of the grain distribution function and increasing discrepancies between the signal decays of successive experiments at different points in the material inevitably occur. In general the FRS signal will decay in a multiexponential way, and the amplitude of each contributing component is given by the statistical weight of the corresponding grains in the orientation distribution inside the sample (or the hologram). Thus FRS decay at the Bragg diffraction position is given by

$$I(t) = [\sum_k \mathbf{E}_k \exp(-t/\tau_k)]^2 \qquad (10)$$

with

$$\tau_k = \mathbf{d}^2/[4\pi^2 \mathbf{D}(\alpha_k)] \qquad (11)$$

where τ_k is the relaxation time for the kth grain with its lamellar normal oriented at an angle α_k with respect to the measuring direction. We should find the characteristics of diffusion as well, namely, the $\mathbf{d}^2$ dependence for the relaxation time for the each component k of the multiexponential decay as long as we really stay in the intermediate scale regime. This might be difficult to realize because in the general case we will have a distribution of grain sizes, so that on increasing the fringe spacing the condition **d** ≪ **L** will become invalid for an increasing number of grains with smaller size.

In these three special cases we were able to discuss the transport without reference to the type of hologram. In the more general case, if we want to incorporate the folding of the lamellae more realistically, the *thin hologram* (sample thickness $B \ll d$) is easier to treat, although it is the more unrealistic picture of the real situation. Because the hologram thickness is much smaller than the fringe spacing, it is possible to solve the scattering problem exactly, following the formalism of Kogelnik's coupled wavey theory.[11] The problem stays in solving the diffusion equation, but once we have determined the concentration distribution of the bleached and unchanged molecules as a function of time in 3D space, this gives us a complex transmission function $T(x,y,t)$ which integrates over the z dependence of the concentration, due to the small sample thickness. Here x is the measuring direction, z is the film normal, and Oxy is the plane parallel to the film surface, while the incident laser beam propagates at an angle $\theta/2$ with respect to the z direction in the plane Oxz. Even if the fringe pattern develops into a complex random pattern after some time of diffusion, caused by anisotropy and confinement of the system, the scattered light intensity at the position of the first-order Bragg peak is always given by the Fourier transform of the complex transmittance function according to eq 12. This integral has to be carried

$$I(t)/I_0 = \frac{1}{A^2}[\int\int T(x,y,t) \exp(i2\pi x/|\mathbf{d}|)\, dx\, dy]^2 \qquad (12)$$

out over the whole area A of the hologram. Compared to the case of an isotropic system, there arises an additional problem in evaluating the signal decay. In the case of the block copolymer system having curved lamellar interfaces, the true starting condition $T(x,y,t) = T(x,t)$ has to be known and it is not sufficient to assume that it is a cosine function, as is generally done for isotropic systems. The true starting condition depends on beam overlap and bleaching conditions and is in fact a Fourier integral, with the dominating Fourier mode giving rise to the diffraction maximum at the detector position. In the isotropic case these Fourier components develop independently so that for simplicity and without mistake we can look only at the first Fourier component. This however is no longer true in the case of the anisotropic diffusion on curved lamellae.

If the lamellae are curved or folded on the length scale **d** (as in Figure 12), this leads to a nonlinear transformation of the diffusion process as we project it on the measuring direction. (In principle this problem is separable into Fourier components, if we could use a coordinate system which is affinely folded with the lamellar planes.) The Fourier components get coupled, and the true starting condition becomes essential to be known. This again is possible to obtain, in principle, by measuring the forced Rayleigh intensity not only at the position of the first-order Bragg peak but as a function of the scattering vector **q**, thus monitoring the whole forced Rayleigh structure factor.

The situation is even worse for the realistic case of a thick hologram. Here the diffusion problem is exactly the same, but the central difficulty is in the scattering problem. The result of the coupled wavy theory as derived by Kogelnik[10,12] to calculate the diffracted light intensity

$$I = I_0 \exp(-KB/\cos\beta)[\sin^2(\pi\Delta nB/\lambda\cos\beta) + \sinh^2(\Delta KB/\lambda\cos\beta)] \qquad (13)$$

of which the first approximation is generally used to evaluate FRS measurements, cannot be applied. In this equation K is the absorption constant, B is the sample

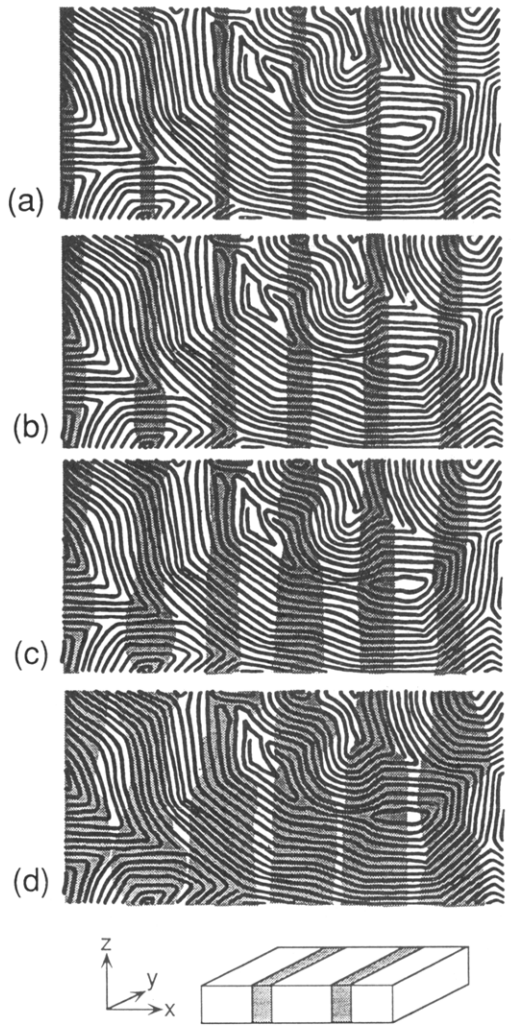

Figure 12. Schematic illustration of the time change in the spatial distribution of labeled polymers indicated by the gray zone: (a) immediately after at $t = 0$, (b) $t = t_1$, (c) $t = 4t_1$, and (d) $t = 9t_1$.

thickness, β is the angle between the incident beam and the normal onto the film surface (i.e., $\beta = \theta/2$), λ is the wavelength of light, and n is the refractive index at this wavelength. Δn and ΔK are amplitudes of a grating-like modulation in terms of refractive index and absorption coefficient. This equation has been derived under the assumption of light waves propagating in a planar grating.[10] This is not at all valid in the general case of diffusion in block copolymers. Caused by the anisotropy of diffusion and the topology of the lamellar microdomains, the initially planar grating is quickly transformed into a more or less random pattern as is tried to visualize in Figure 12. In this figure we start from the most simple initial concentration pattern (a): the fringes of labeled material are assumed to be infinitely thin planes parallel to the Oyz plane, periodically ordered along the x direction (part a). We show the mean displacement after times t_1, $4t_1$, and $9t_1$, respectively in parts b–d, to indicate how a concentration front would develop with time for a particular spatial arrangement of the lamellar microdomains. Here $D_\perp$ is again assumed to be negligibly small. Because of the twisting and bending of the lamellae, the inhomogeneity of the grating which is visualized in the x direction must occur also in the z direction. It can be seen from Figure 12 that a twisting and bending of the lamellae will not only deform the fringes irregularly but may even cause a local shift in the center position of the fringe. This is because transport into the $+x$ and $-x$ directions may be of different speed if the lamellar interface is bent at the position of the fringe. Thus produced concentration pattern is obviously very complex and far apart from the planar dielectric grating assumed in the standard theory.[10,12] The situation is much closer to the problem of Mie scattering[13] from an absorbing and strongly fluctuating system which is yet unresolved.

V. Concluding Remarks

We can conclude from the considerations given in section IV that further development of theories concerning the transport in confined, folded, or topologically complicated systems is highly desirable. Such systems can be realized quite easily in modern materials, and methods for diffusional studies are available. Furthermore the development of a more extensive theory of forced Rayleigh scattering, covering, e.g., the scattering from nonplanar, slightly wavy gratings, seems necessary to permit a more thorough evaluation of contemporary measurements.

It is clear, from the above discussion, that the lack of comprehensive theories is most seriously felt in the case of strongly folded or twisted lamellae systems. We may conclude from the TEM micrograph shown in Figure 4 and the method of sample preparation that the lamellae in the presently studied system are not folded in such a strong way. It may be described with some confidence by wavy planar lamellae, at least up to the largest diffusional length scale of 14 μm. Thus the evaluation of the FRS measurements in section III will still be meaningful. The rather large grains, which we tried to prepare in terms to show the diffusional anisotropy directly, prohibit at the same time that we reach the range of macroscopic scale experiments, even with the largest fringe spacing. Thus the most reasonable of the three solvable model experiments seems to be the intermediate scale experiment. In reality for most of the fringe spacings we are in the region between intermediate and macroscopic scale: grains and fringes are of similar size. For the smallest fringe spacings around 200 nm the intermediate scale looks quite reasonable. However, looking at Figure 4 over the whole sample thickness of 50 μm, the orientation of the lamellae cannot be assumed to stay constant. Because of this, the planar fringes will develop into wavy fringes, but probably without the extreme features of Figure 12. Simply speaking, the main reason why a more thorough evaluation according to eqs 6 and 7, which would permit a comparison with the structural anisotropy, is not valid is that the orientational variation of the lamellar normals $\mathbf{n}(\mathbf{r})$ makes a complex transmission function $T(x,y,t)$ after some time of diffusive decay.

Acknowledgment. D.E. acknowledges gratefully the financial support by Japan Society for the Promotion of Science (JSPS) and Alexander von Humboldt-Stiftung (AvH). A part of this work was supported by Grants-in-aid for Encouragement of Young Scientists-A from Ministry of Education, Science and Culture, Japan (02953046 and 02963006 offered to M.T. and D.E., respectively). We are thankful to Prof. H. Sillescu, Prof. M. Doi, Prof. A. Onuki, Dr. J. Harden, and Dr. T. Pakula for helpful discussions and comments, to Dr. M. Antonietti, Universität Mainz, for the synthesis of the block copolymers, to Mr. K. Kimishima for the fractionation of the block copolymers, and to Mr. S. Koizumi for help with TEM observation.

References and Notes

(1) Shull, K.; Kramer, E. J.; Bates, F. S.; Rosedale, J. H. *Macromolecules* **1991**, *24*, 1383.

(2) Fredrickson, G. H.; Milner, S. T. *Mater. Res. Soc. Symp. Proc.* **1990**, *177*, 169.
(3) Annighoefer, F.; Gronski, W. *Makromol. Chem., Rapid Commun.* **1983**, *4*, 123. Hashimoto, T.; Nagatoshi, K.; Todo, A.; Hasegawa, H.; Kawai, H. *Macromolecules* **1974**, *7*, 364. Hashimoto, T.; Todo, A.; Itoi, H.; Kawai, H. *Macromolecules* **1977**, *10*, 377. Hashimoto, T.; Shibayama, M.; Kawai, H. *Macromolecules* **1980**, *13*, 1237.
(4) Hadziioannou, G.; Mathis, A.; Skoulios, A. *Colloid Polym. Sci.* **1979**, *257*, 136.
(5) Ehlich, D.; Takenaka, M.; Hashimoto, T. *Macromolecules*, in press (1993), part of this series. We are very thankful to Prof. H. Sillescu, Universität Mainz, for temporarily supplying components and drawings of his FRS setup. Sillescu, H.; Ehlich, D. In *Application of Laser in Polymer Science and Technology*; CRC: Boca Raton, FL, 1989.
(6) Pakula, T.; Saijo, K.; Kawai, H.; Hashimoto, T. *Macromolecules* **1985**, *18*, 1294.
(7) Saijo, K.; Okamoto, S.; Kimishima, K.; Kume, T.; Hashimoto, T. *Polym. Prepr., Jpn.* **1990**, *39*, 383. Okamoto, S.; Saijo, K.; Kimishima, K.; Kume, T.; Hashimoto, T. *Polym. Prepr., Jpn.* **1990**, *39*, 384. Hashimoto, T.; Saijo, K.; Kume, T.; Kimishima, K.; Okamoto, S., in preparation.
(8) Okamoto, S.; Ehlich, D.; Hashimoto, T., In preparation.
(9) Antonietti, M.; Coutandin, J.; Ehlich, D.; Sillescu, H. In *Physical Optics of Dynamic Phenomena and Processes in Macromolecular Systems*; Sedlacek, B., Ed.; de Gruyter: Berlin, 1985; p 191.
(10) Eichler, H. J.; Guenther, P.; Pohl, D. W. *Laser Induced Dynamic Gratings*; Springer-Verlag: Berlin, 1986.
(11) Hashimoto, T.; Nagatoshi, K.; Todo, A.; Hasegawa, H.; Kawai, H. *Macromolecules* **1974**, *7*, 364. Hashimoto, T.; Shibayama, M.; Kawai, H. *Macromolecules* **1980**, *13*, 1237.
(12) Kogelnik, H. *Bell. Syst. Technol. J.* **1969**, *48*, 2909.
(13) Mie, G. *Ann. Phys.* **1908**, *25*, 377. See, for example: Van de Hulst, H. C. *Light Scattering by Small Particles*; Wiley & Sons., Inc.: New York, 1957. Kerker, M. *Scattering of Light and Other Electromagnetic Radiation*; Academic Press: New York, 1969.

Registry No. SI (block copolymer), 105729-79-1.